First-principles investigations of orbital magnetic moments and electronic structures of the double perovskites Sr_2FeMoO_6, Sr_2FeReO_6, and Sr_2CrWO_6

Horng-Tay Jeng
Physics Division, National Center for Theoretical Sciences, Hsinchu 30043, Taiwan

G. Y. Guo
Department of Physics, National Taiwan University, Taipei 106, Taiwan
and National Synchrotron Radiation Research Center, Hsinchu 300, Taiwan

(Received 16 September 2002; revised manuscript received 2 January 2003; published 31 March 2003)

The electronic structures and magnetic properties of double perovskites Sr_2FeMoO_6, Sr_2FeReO_6, and Sr_2CrWO_6 have been studied by using the full-potential linear muffin-tin orbital method within the local-spin-density approximation (LSDA) and the generalized gradient approximation (GGA). The on-site Coulomb energy U has also been taken into account in both schemes (LSDA+U and GGA+U). The results predict a half-metallic ferrimagnetic band structure with total spin magnetic moment of $4\mu_B$, $3\mu_B$, and $2\mu_B$ per formula unit for Sr_2FeMoO_6, Sr_2FeReO_6, and Sr_2CrWO_6, respectively. By including the spin-orbit coupling in the self-consistent calculations, we find that the $5d$ transition-metal atoms W and Re exhibit large unquenched orbital magnetic moments because of significant spin-orbit interaction in $5d$ orbitals. On the other hand, in Fe and Cr $3d$ and Mo $4d$ orbitals, the orbital moments are all quenched even though the on-site Coulomb energy U is taken into account. This is in strong contrast to the enhanced large $3d$ orbital moments in CoO and NiO but similar to the quenched orbital moment in CrO_2.

DOI: 10.1103/PhysRevB.67.094438 PACS number(s): 31.15.Ar, 71.20.−b, 32.10.Dk

I. INTRODUCTION

Double perovskites, discovered in the 1960s,[1] are a broad class of compounds with a chemical formula of $A_2BB'O_6$,[2] where A is an alkaline-earth-metal or rare-earth-metal ion and B and B' are transition-metal ions. Recently, ordered Sr_2FeMoO_6 (Ref. 3) and Sr_2FeReO_6 (Ref. 4) attract renewed attention because of the intrinsic tunneling-type magnetoresistance found at room temperature. Band-structure calculations reveal that they are ferrimagnetic half-metals with highly spin-polarized transport properties at the Fermi level.[3,4] Both Curie temperatures are found to be fairly high (T_C=415 and 401 K, respectively), making them potential materials for industrial applications in magnetoresistive devices as well as in spintronics at room temperature. Apart from these extensively investigated iron-based double perovskites, recently a chromium-based double perovskite Sr_2CrWO_6 has also been found to exhibit a large low-field magnetoresistance and a high Curie temperature of 390 K.[5] It is therefore interesting to study comparatively the electronic structures and both spin and orbital magnetic moments of these materials.

Double perovskite ($A_2BB'O_6$) crystallizes in the rocksalt structure (Fig. 1) with alternate perovskite units ABO_3 and $AB'O_3$ along three crystallographical axes. The corners of each perovskite unit are in turn occupied by transition-metal atoms B and B' with oxygen atoms located in between, forming alternate BO_6 and $B'O_6$ octahedra. The large alkaline-earth-metal atom A occupies the body-centered site with a 12-fold oxygen coordination in each unit. In the ionic model, the transition-metal ions are in the $(BB')^{8+}$ valence state. In Sr_2FeMoO_6 and Sr_2FeReO_6, where $Fe^{3+}(3d^5)$ are in the high spin state of S=5/2 according to Hund's rule, $Mo^{5+}(4d^1)$ and $Re^{5+}(5d^2)$ are highly ionized with valence spin states of $S=\frac{1}{2}$ and S=1, respectively. The resultant total spin magnetic moments for the ferrimagnetic states are thus $4\mu_B$ and $3\mu_B$ per formula unit (f.u.), respectively. In Sr_2CrWO_6, the valence configurations are $Cr^{3+}(3d^3)$ and $W^{5+}(5d^1)$. Consequently, the total moment is $2\mu_B/Sr_2CrWO_6$ for the ferrimagnetic ground state. The observed saturation magnetizations for Sr_2FeMoO_6, Sr_2FeReO_6, and Sr_2CrWO_6 are $4\mu_B$/f.u. at 10 K,[6] $2.7\mu_B$/f.u. at 4.2 K,[4] and $\sim 1\mu_B$/f.u. at low temperature,[5] respectively. The smaller saturation magnetizations observed in experiments are probably related to the mis-site-type disorder of the transition-metal sites. Monte Carlo simulations also suggested that the mis-site defect could account for the reduction of magnetization.[7]

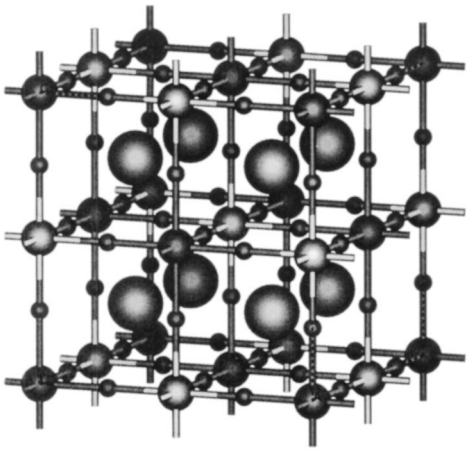

FIG. 1. Crystal structure of double perovskite. Big and small balls denote Sr and O, respectively. Middle light and middle dark balls denote the two different transition-metal atoms, respectively.

The ordered double perovskite Sr_2FeMoO_6 has been demonstrated to exhibit a ferrimagnetic half-metallic ground state[3] by using the ultrasoft pseudopotential method. It was suggested that the antiferromagnetic superexchange interaction between Fe $3d^5$ $S=\frac{5}{2}$ and Mo $4d^1$ $S=\frac{1}{2}$ spins would produce a large ferrimagnetic magnetization.[3] The Fermi level falls in an energy gap in the majority spin, whereas in the minority spin, the hybridized t_{2g} bands of Fe $3d$ and Mo $4d$ orbitals at the Fermi energy give rise to the fully spin-polarized conductivity. Using the full-potential (FP) augmented plane-wave method, the electronic structure of Sr_2FeReO_6 has also been found to be fairly similar to that of Sr_2FeMoO_6, indicating that the ferrimagnetic half-metallic ground state is a generic feature for a broad class of the ordered double perovskite.[4] With a combined *ab initio* and model Hamiltonian approach, the strongly enhanced effective exchange at Mo site due to the Fe($3d$)-Mo($4d$) hybridization was suggested to be responsible for the fundamental mechanism of the high Curie temperature in Sr_2FeMoO_6.[8] Based on detailed electronic structure calculations using the local-spin-density approximation with on-site Coulomb energy (LSDA+U) method,[9] a more general idea was proposed that a nonmagnetic element located at the midpoint of neighboring high-spin $3d$ elements stabilizes the ferromagnetic coupling of the $3d$ elements.[10] Electronic structures from a full-potential linearly combined atomic-orbital band method also demonstrated that the half-metallic character is not caused by direct Mo-Mo interactions but by indirect Mo-O-Fe-O-Mo pdd-π couplings, which are simultaneously responsible for their ferrimagnetic character.[11] An x-ray absorption spectroscopy with linearly and circularly polarized photons suggests that instead of the conventional double-exchange mechanism, the delocalized Mo $4d$ spin density over several sites gains a stronger antiferromagnetic coupling to the localized up spins at the Fe site, yielding a new origin of the ferrimagnetic ground state for Sr_2FeMoO_6.[12] On the other hand, the frequently believed ferrimagnetic half-metallic ground state was argued to be unstable because of the competition between the generalized double-exchange mechanism, operating in the hybridized t_{2g} bands of Fe $3d$ and Mo $4d$ orbitals in the metallic minority-spin channel, and the strong antiferromagnetic superexchange interactions in the Fe sublattice, mediated by virtual electron hopping into the unoccupied Mo $4d$ states.[13] Possible mechanisms responsible for a stable magnetic ground state such as spin-spiral ordering, spin canting, breathing distortion, and disorder, as well as antisite defects were also discussed in Ref. 13.

In this work we report systematic investigations on the orbital contributions to the magnetic moments and on the electronic structures of the extensively studied Fe-based double perovskites Sr_2FeMoO_6 and Sr_2FeReO_6 and the newly found Cr-based double perovskite Sr_2CrWO_6 (Ref. 5) within the LSDA and generalized gradient approximation (GGA). The on-site Coulomb energy U has also been taken into account in both schemes (LSDA+U and GGA+U) to unravel the correlation effects of the localized d orbitals on the orbital magnetic moments as well as on the electronic structures. In the following section, we briefly summarize the computational details. The calculated orbital magnetic moments and electronic structures are discussed in detail in Sec. III. The conclusions are given in Sec. IV.

II. COMPUTATIONAL DETAILS

The relativistic all-electron full-potential linear muffin-tin orbital method[14] (FP-LMTO) including the spin-orbit interaction was used to perform self-consistent band-structure calculations within both the LSDA and LSDA+U schemes.[15] The Vosko-Wilk-Nusair parametrization[16] and also GGA[17] for the exchange-correlation potential were used in the calculations. For cubic (space group $Fm3m$, No. 225) Sr_2FeReO_6 and Sr_2CrWO_6, we used the experimental lattice parameters of 7.89 Å (Ref. 18) and 7.832 Å (Ref. 5), respectively. While for tetragonal Sr_2FeMoO_6 (space group $I4/mmm$, No. 139), the lattice constants were $a=7.878$ Å and $c/a=1.001$.[3] The radii of the muffin-tin spheres for Sr and O were $3.5a_0$ and $1.5a_0$ (Bohr radius), respectively. While for transition-metal atoms (Fe, Cr, Mo, W, and Re), the radii of muffin-tin spheres were $2.0a_0$. A single-κ LMTO basis set expanded in spherical harmonics up to angular momentum $l=6$ was used for the valence-band charge densities and potentials inside the nonoverlapping muffin-tin spheres. While in the interstitial region, more than 14 500 plane waves with energies up to 100 Ry were included in the calculations. In band-structure (BS) and density of states (DOS) calculations, 72 and 163 k points were used for cubic Sr_2FeReO_6 and Sr_2CrWO_6 and for tetragonal Sr_2FeMoO_6, respectively. For the [001] direction of magnetization, in which the spin-orbit coupling turned the two cubic systems into tetragonal symmetry, the number of k points used was 242 over the irreducible wedge of the tetragonal Brillouin zone. To explore the effects of the on-site Coulomb energy U on the electronic structures and the magnetic moments, we used U of 4 eV (Ref. 19) and 3 eV (Ref. 20) and exchange interaction parameter J of 0.89 eV (Ref. 9) and 0.87 eV (Ref. 20) for Fe and Cr, respectively, in the LSDA+U and GGA+U calculations.

III. RESULTS AND DISCUSSION

Figure 2 illustrates the DOS of Sr_2FeMoO_6 (upper panel), Sr_2FeReO_6 (middle panel), and Sr_2CrWO_6 (lower panel) from GGA calculations. The obtained results of Sr_2FeMoO_6 and Sr_2FeReO_6 agree well with published works.[3,4,10] In the majority spin, the Fermi energy falls in an energy gap between the occupied Fe e_g bands and the unoccupied Mo(Re) t_{2g} bands. Since the energy gap in the majority spin results from the antiferromagnetic coupling between Fe and Mo(Re), it may be called an antiferromagnetic coupling gap in consistence with the mechanism proposed in Ref. 10. In contrast, in the minority spin, the Fermi level lies in the partially filled t_{2g} bands of Fe $3d$, Mo $4d$ (Re $5d$), and O $2p$ hybridized states. The spin states of Mo ($S=\frac{1}{2}$) and Re($S=1$) ions couple antiferromagnetically to the high-spin states of Fe ions, resulting in a ferrimagnetic half-metallic ground state. The mechanism of the ferrimagnetic coupling is attributed to the Fe(t_{2g})-O($2p_\pi$)-Mo(Re)(t_{2g}) hybridization.[11] Since the up-spin Fe $3d$ bands are nearly

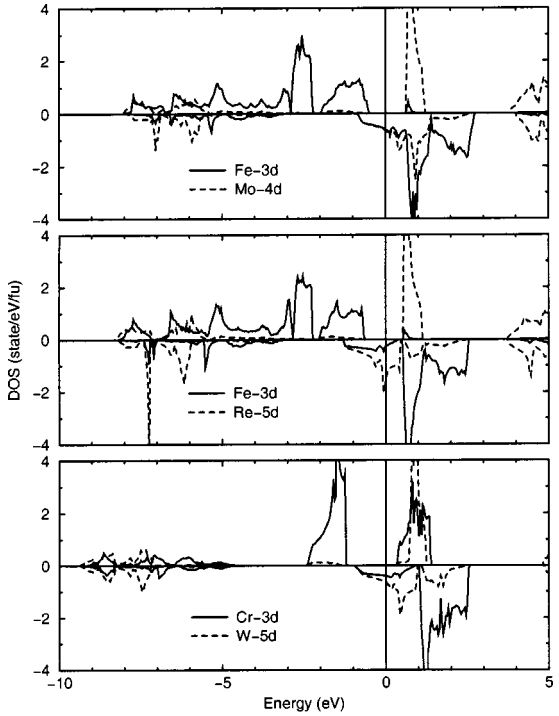

FIG. 2. Density of states of Sr_2FeMoO_6 (upper panel), Sr_2FeReO_6 (middle panel), and Sr_2CrWO_6 (lower panel) from the GGA. The Fermi level is at zero energy.

closed and the down-spin Fe $3d$ bands are partially occupied, only the down-spin Mo(Re) t_{2g} orbital would hybridize with the open down-spin Fe t_{2g} orbital for lowering the kinetic energy.

It can be seen in Fig. 2 that the DOS of Cr-based Sr_2CrWO_6 are different from the DOS of Fe-based compounds mentioned above. The O $2p$ bands are at a much lower bonding energy from 4 to 9 eV below the Fermi level, whereas the higher antibonding $3d$ e_g bands of Cr are located at about 1 eV above the Fermi energy in the majority spin. The stronger bonding-antibonding splitting results from the similar nearest-neighbor distances and relatively larger Cr $3d$ orbital as compared to those of Fe in Sr_2FeMoO_6 and Sr_2FeReO_6. Similarly the octahedral ligand field splittings ($\sim$2 eV) between the occupied t_{2g} and unoccupied e_g states of Cr $3d$ bands are larger than those in Fe $3d$ bands. The Fermi level thus falls in the crystal-field-splitting gap in the majority spin. This is in contrast to the energy gap at the Fermi level between Fe $3d$ and Mo $4d$ (Re $5d$) bands in Fe-based double perovskite Sr_2FeMoO_6 (Sr_2FeReO_6). In the minority spin, the Fermi level lies in the partially filled Cr $3d$ and W $5d$ hybridized t_{2g} bands. The obtained exchange splitting of $\sim$2 eV in Cr $3d$ bands is smaller due to the valence configuration $Cr^{3+}(3d^3)$ of less electrons and weaker Hund's coupling. Also the induced exchange splitting in the W $5d$ orbital is smaller than that in Re $5d$ of Sr_2FeReO_6. The magnetism of Sr_2CrWO_6 is similar to that in Sr_2FeMoO_6 and Sr_2FeReO_6. The difference is that the up-spin Cr t_{2g} band rather than the up-spin Fe $3d$ band is filled. Only the down-spin W t_{2g} orbital would hybridize with the open down-spin Cr t_{2g} orbital, yielding an antiferromagnetic coupling between Cr and W. The results indicate that in addition to the same ferrimagnetic ground states, Sr_2CrWO_6 is a crystal-field-gap half-metal, whereas Sr_2FeMoO_6 and Sr_2FeReO_6 are antiferromagnetic-coupling-gap half-metals.

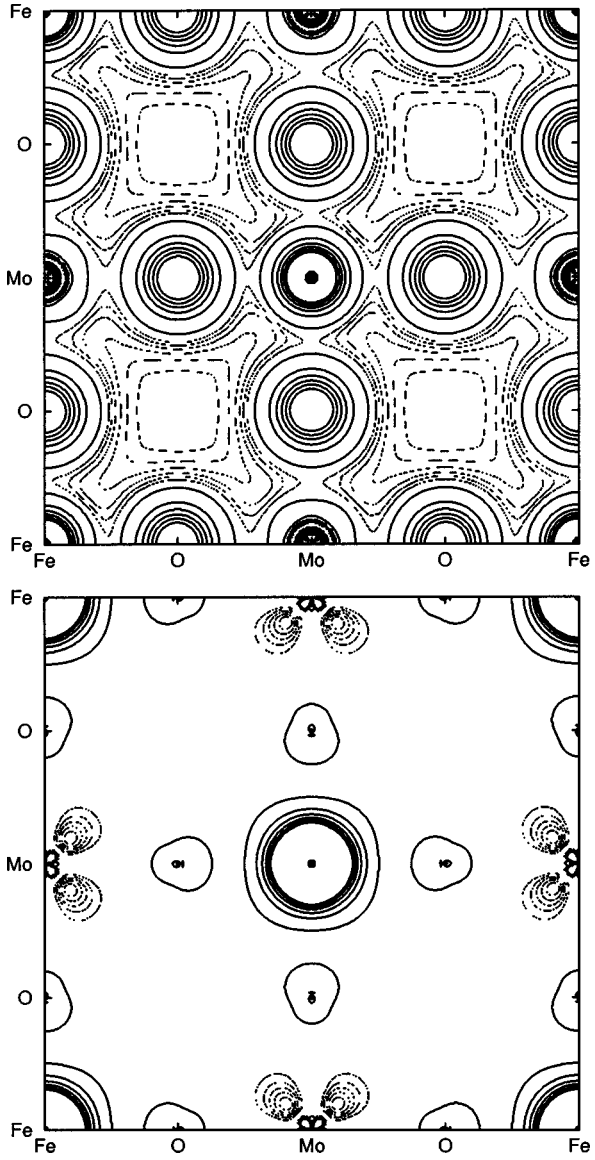

FIG. 3. Valence charge (upper panel) and spin (lower panel) densities of Sr_2FeMoO_6 from the GGA. In the upper panel, the contours are along equal charge density lines from 0.015 to $0.065/a_0^3$ (broken lines) with step $0.01/a_0^3$, and from 0.1 to $0.85/a_0^3$ (solid lines) with step $0.15/a_0^3$. In the lower panel, they are from -0.005 to $-0.03/a_0^3$ (broken lines) with step $-0.005/a_0^3$, and from 0.01 to $0.16/a_0^3$ (solid lines) with step $0.03/a_0^3$.

Figures 3 and 4 show the valence charge (upper panels) and spin (lower panels) density contours of Sr_2FeMoO_6 and Sr_2CrWO_6, respectively, from the GGA. It can be seen in Fig. 3 that charge distributions at Fe sites are nearly spherical because of nearly half-filled Fe $3d$ orbitals. Those Fe $3d$ electrons that are more than half full have moved to oxygen sites for stabilizing the ground state. Also, most of the loosely bounded Mo $4d$ electrons with larger orbitals have

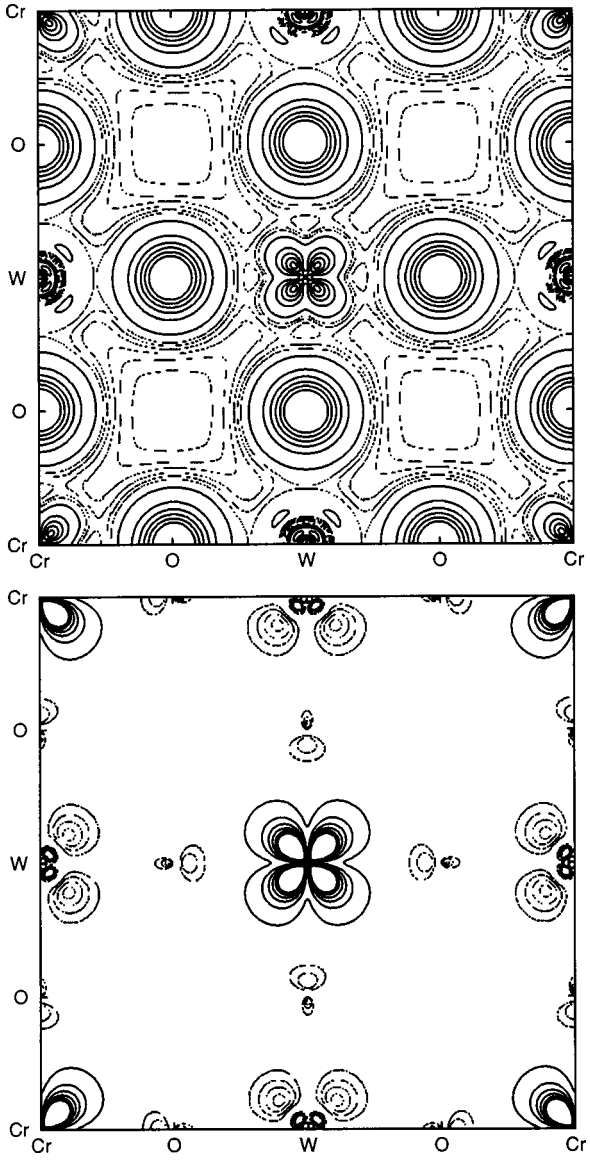

FIG. 4. Valence charge (upper panel) and spin (lower panel) densities of Sr_2CrWO_6 from the GGA. In the upper panel, the contours are along equal charge density lines from 0.015 to $0.065/a_0^3$ (broken lines) with step $0.01/a_0^3$, and from 0.1 to $0.85/a_0^3$ (solid lines) with step $0.15/a_0^3$. In the lower panel, they are from -0.005 to $-0.03/a_0^3$ (broken lines) with step $-0.005/a_0^3$, and from 0.01 to $0.16/a_0^3$ (solid lines) with step $0.03/a_0^3$.

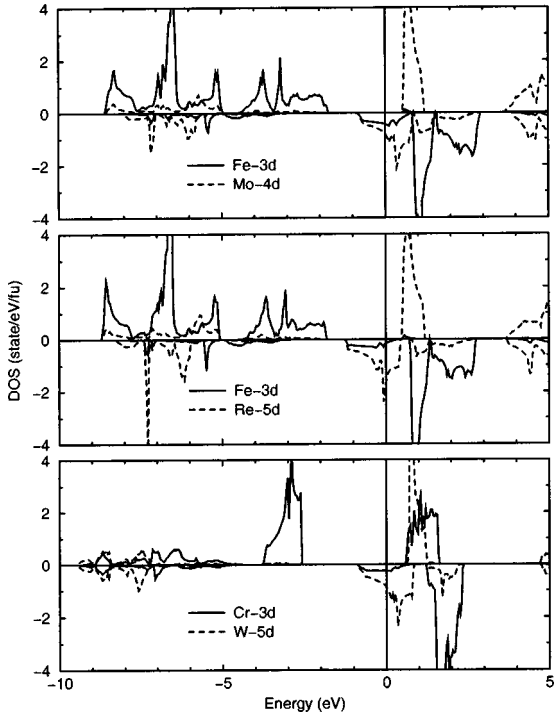

FIG. 5. Density of states of Sr_2FeMoO_6 (upper panel), Sr_2FeReO_6 (middle panel), and Sr_2CrWO_6 (lower panel) from GGA+U. The Fermi level is at zero energy.

spread out, leaving the highly ionized Mo atoms. The oxygen atoms with high electron affinities therefore attract these electrons together with the itinerant Fe 4s and Mo 5s electrons to form nearly closed O 2p shells with spherically distributed charge densities. Note that the size of the nearly closed-shell oxygen ions are slightly larger than the size of iron ions with nearly half-filled 3d orbitals. The charge distributions also show that there exists no direct interaction between two nearest Fe-Fe or Mo-Mo pairs, whereas along each Fe-O-Mo-O-Fe chain, the hybridizations between Fe 3d, O 2p, and Mo 4d orbitals are fairly significant.[11] On the other hand, the spin density distribution of Sr_2FeMoO_6 (lower panel of Fig. 3) also demonstrates that the spin moments of Fe and Mo are mainly localized at nuclear sites and are coupled antiferromagnetically. This is different from the model proposed in Ref. 12 in which the Mo 4d spin densities are delocalized over several sites. The roughly spherical distributed positive spin densities at Fe sites indicate the nearly half-filled 3d orbitals. While the occupied Mo 4d orbital is mainly composed of down-spin t_{2g} electrons. The charge and spin density distributions in Sr_2FeReO_6 are basically the same as those in Sr_2FeMoO_6, and are not shown here. As for Sr_2CrWO_6 (Fig. 4), the e_g electrons of Cr 3d orbitals and most of the W 5d electrons have moved to oxygen sites forming O 2p closed shells. Only the 3d t_{2g} orbitals of Cr are occupied for lowering the ground-state energy. Furthermore, the hybridizations are still along the Cr-O-W-O-Cr chain, and no direct interaction between Cr-Cr and W-W pairs are found. The spin moments of Cr t_{2g} and W t_{2g} are mainly localized and couple antiferromagnetically as shown in the lower panel of Fig. 4, resulting in a ferrimagnet.

Taking the on-site Coulomb interaction U into account, the occupied Fe 3d and Cr t_{2g} bands in the majority spin are drastically pushed downwards as shown in Fig. 5. Consequently the energy gaps are strongly enhanced. Interestingly, the unoccupied spin-up Cr e_g, Mo 4d, and W(Re) 5d bands remain more or less the same. In the minority spin, the 3d t_{2g} bands of Fe and Cr move upwards slightly, whereas the t_{2g} bands of Mo 4d and W(Re) 5d orbitals are lowered slightly. The antiferromagnetic coupling between Fe and Mo(Re) and between Cr and W is thus strengthened. The relative shifts in majority and minority spin bands induced by the on-site Hubbard repulsion U therefore stabilize the ferrimagnetic half-metallic ground states. Notably, electronic

TABLE I. Spin and orbital magnetic moments (μ_B/atom) of Sr_2FeMoO_6, Sr_2FeReO_6, and Sr_2CrWO_6.

	Spin		Orbital	
Sr_2FeMoO_6	Fe	Mo	Fe	Mo
GGA	3.80	−0.33	0.043	0.032
GGA+U	3.96	−0.43	0.047	0.045
LSDA	3.74	−0.28	0.047	0.028
LSDA+U	3.91	−0.39	0.054	0.042
Sr_2FeReO_6	Fe	Re	Fe	Re
GGA	3.81	−0.85	0.070	0.23
GGA+U	3.98	−0.96	0.066	0.27
LSDA	3.72	−0.74	0.083	0.21
LSDA+U	3.91	−0.85	0.077	0.26
Sr_2CrWO_6	Cr	W	Cr	W
GGA	2.30	−0.33	−0.007	0.10
GGA+U	2.46	−0.45	−0.007	0.15
LSDA	2.20	−0.27	−0.017	0.08
LSDA+U	2.42	−0.41	−0.018	0.13

structures (BS and DOS) and magnetic moments (spin and orbital moments as discussed below) of the three considered double perovskites from the LSDA are basically similar to those from the GGA. Including the on-site U in LSDA calculations (LSDA+U) also yields similar band dispersions and magnetic moments as those from GGA+U. In this work, we have also calculated the theoretical lattice constants for these double perovskites by using LSDA and GGA. Since GGA gives better lattice constants for these double perovskites (~1% smaller than the experimental lattice constants), we present here the GGA and GGA+U results only. It has been demonstrated for Ba_2FeMoO_6 that the LSDA+U calculation yields better agreement with experiment in the spectral peak positions than does the LSDA calculation.[21] However, during this work, we were not aware of suitable experimental spectra to examine the correctness of the obtained DOS from the GGA and from the GGA+U for these Sr-based double perovskites.

The calculated spin and orbital magnetic moments from the GGA (LSDA) and from the GGA+U (LSDA+U) for Sr_2FeMoO_6, Sr_2FeReO_6, and Sr_2CrWO_6 are listed in Table I. For the most extensively studied compound Sr_2FeMoO_6, the GGA gives spin moments of 3.80 and $-0.33\mu_B$/atom for Fe and Mo, respectively. The obtained moments agree well with published results from first-principles calculations.[10] Also they are consistent with measured spin moments of Sr_2FeMoO_6 ranging from 3.1 to $4.5\mu_B$/Fe and from 0 to $-0.5\mu_B$/Mo.[22–27] Because of the diffusive $5s$ valence configuration and the ionic behavior of the alkaline-earth-metal element, the local moments of Sr ions are negligibly small. The spin moments on the oxygen ions are also small due to the nearly closed $2p$ shells. The resultant total spin moment of the half-metallic ground state is $4.00\mu_B$/f.u., being consistent with that from the ionic viewpoint and from the experimental observation.[6] On the other hand, the orbital magnetic moment of Fe $3d$ orbital is of the same sign as the spin moment, indicating that the $3d$ orbital is over half-filled in accordance with Hund's rule. Due to the octahedral ligand field, the orbital moment is only $0.043\mu_B$/Fe. In the highly ionized $Mo^{5+}(4d^1)$ state, as a consequence of Hund's rule, the orbital moment aligns antiparallel to the spin moment. The orbital moment of $0.032\mu_B$/Mo is rather small in spite of the stronger spin-orbit interaction in the $4d$ orbital. This results from the larger size of the $4d$ orbital and thus the enhanced crystal field. For Sr $5s$ and O $2p$ orbitals, the orbital moments are negligibly small.

In Sr_2FeReO_6 (Table I), the spin moment of Fe from the GGA is similar to that in Sr_2FeMoO_6, while the orbital moment is larger. The alignments of spin and orbital moments in Sr_2FeReO_6 are the same as those in Sr_2FeMoO_6. Because of the additional $5d$ electron of Re, the induced spin moment of $-0.85\mu_B$/Re is much larger than that of Mo, resulting in a smaller total spin moment of $3.00\mu_B$/f.u. Remarkably, even in GGA calculations, Re exhibits large unquenched orbital moment of $0.23\mu_B$/atom due to strong spin-orbit coupling in $5d$ orbital. This is in contrast to the well-known trend that the LSDA and GGA usually give quenched orbital moments for transition-metal oxides.[28] The overestimated quenching effect results from the spurious self-interaction presented in the LSDA and GGA.[29] As a result, the LSDA and GGA give more diffusive d orbitals accompanied by stronger crystal fields. The spurious self-interaction in the LSDA and GGA also causes an evenly distributed occupation among the five-fold d orbitals for lowering the Coulomb energy. The strong spin-orbit coupling of $5d$ orbital is about 4 times larger than that of $3d$ orbital. As a result, the LSDA and GGA give large unquenched orbital moments for Re in spite of the spurious self-interaction.

Due to the valence configuration $Cr^{3+}(3d^3)$ of fewer electrons, the spin moment of $2.30\mu_B$/Cr in Sr_2CrWO_6 from the GGA is much smaller than those in the Fe-based double perovskites (Table I). The induced spin moment of $-0.33\mu_B$/W is the same as that of Mo and much smaller than that of Re. The resultant total spin moment is only $2.00\mu_B/Sr_2CrWO_6$. On the other hand, the orbital moment of $-0.007\mu_B$/Cr is almost fully quenched. This could be understood as a consequence of stronger ligand field caused by the relatively larger size of the Cr $3d$ orbital as compared with the Fe $3d$ orbital. Consistent with Hund's rule for a Cr $3d$ orbital less than half-full, the orientation of the orbital moment is antiparallel to the spin moment. For tungsten, the orbital size and crystal field, as well as the spin-orbit coupling strength, are similar to those of Re. The orbital moment per electron is therefore expected to be similar to that of Re. Due to fewer valence $5d$ electrons and down-spin occupancies (a half of Re from ionic viewpoint), the obtained orbital moment of $0.10\mu_B$/W is about a half of that of Re.

Taking the on-site Coulomb energy U into account (GGA+U), the spin moments of all the transition-metal atoms are, as expected, enhanced due to charge localization and enhanced exchange integral (Table I). In general, the on-site U slightly enhances the orbital moments of transition-metal ions in double perovskites because of stronger orbital

polarization in *d* orbitals. However, the orbital moment of Fe in Sr_2FeReO_6 is suppressed by the Hubbard repulsion *U*. The reduction of the Fe $3d$ orbital moment indicates a $3d$ orbital closer to half full of zero orbital moment in accordance with the Hund's rule. Note that the orbital moments of $3d$ ions Fe and Cr are all quenched in GGA+*U* calculations. This is in strong contrast to the large unquenched orbital moments of Co and Ni ions in CoO (Ref. 28) and NiO (Ref. 30), respectively, but similar to the quenched orbital moment of Cr in CrO_2 (Ref. 31). The quenched orbital moment of Fe in double perovskites is partly due to the nearly half-filled Fe $3d$ orbital and partly due to the shorter Fe-O distance of $\sim 3.7a_0$ as compared with that of $(3.9–4.1)a_0$ in FeO, CoO, and NiO. As for Cr, due to the more itinerant character of the Cr $3d$ orbital, the orbital moment is quenched even though the on-site Coulomb repulsion *U* is included.[31] On the other hand, the unquenched large orbital moment of Re from the GGA is further enhanced by on-site *U*. This is also the case in the $5d$ element W in Sr_2CrWO_6.

It has been observed that relative to LSDA results, the GGA gives slightly larger spin moments while slightly smaller orbital moments for half-metallic $3d$ transition-metal oxides CrO_2.[31] For the three double perovskites studied in this work, similar trends are also observed in $3d$ elements Fe and Cr (Table I). In contrast, for $4d$ elements Mo and $5d$ ions Re and W, the magnitude of both the spin and orbital moments are enhanced by the GGA. Since no consensus on the measured spin moment have been obtained,[22–27] and also to our knowledge, no orbital moment has been measured, it is still an open question which approximation gives a better description for these double perovskites. Future measurements would clarify this issue.

To unravel the origin of the large orbital magnetic moments in Sr_2FeReO_6 and Sr_2CrWO_6, we calculated the occupation numbers of *d* orbitals projected onto different magnetic orbitals (*m*) for [001] magnetization. The occupation numbers in both spins of Fe $3d$ orbitals from the GGA as well as from GGA+*U* are distributed evenly among the five magnetic orbitals and thus contribute to orbital moments insignificantly. For both spins of Cr $3d$ orbitals, the occupation numbers in $|m|=2$ and in $|m|=1$ magnetic orbitals are nearly equal, separately. Consequently the orbital moments in Cr are quenched. These paired occupancies are attributed to the strong octahedral ligand field and the fewer valence electrons in Cr $3d$ orbitals. On the other hand, due to the strong spin-orbit couplings in $5d$ orbitals of Re and W with heavier nuclei, the down-spin occupancies are not evenly distributed among the fivefold magnetic orbitals. It can be seen in Table II that even from the GGA, the differences in occupation numbers of down-spin $|m|=1$ and $|m|=2$ states of Re $5d$ orbitals are $0.16e$ and $0.08e$, respectively. As a result, the Re $5d$ orbital down-spin states are highly polarized in spite of the octahedral ligand field, leading to a large unquenched orbital magnetic moment (Table I). Taking the on-site *U* into account (GGA+*U*), the orbital polarizations in Re- and W $5d$ orbitals are further enhanced. As shown in Table II, there is a strong tendency to occupy the $m=1$ magnetic orbitals in Re and W $5d$ states. Such a tendency is attributed to the competition between the spin-orbit interaction, which favors larger positive *m* orbitals for down-spin electrons, and the octahedral crystal field, which lowers the energies of t_{2g} ($|m|=1$) states. Figure 6 illustrates the radial charge density distributions of down-spin Re $5d$ (upper panels) and of down-spin W $5d$ (lower panels) orbitals from the GGA (left panels) and from the GGA+*U* (right panels). In all cases shown here, the $m=1$ magnetic orbitals are of the lowest combined spin-orbit and crystal-field energies and are thus the most preferable states. The occupancies in $m=2$ orbitals of lower spin-orbit energies and in $m=-1$ orbitals of lower crystal-field energies are about the same, whereas $m=0$ states are of the lowest occupancies. The on-site *U*

TABLE II. Magnetic-orbital-decomposed occupation number (*e*) of Re and W $5d$ orbitals for [001] magnetization in Sr_2FeReO_6 and Sr_2CrWO_6.

		$m=-2$	$m=-1$	$m=0$	$m=1$	$m=2$
$Re_\uparrow$	GGA	0.27	0.21	0.28	0.20	0.22
$Re_\uparrow$	GGA+*U*	0.26	0.20	0.27	0.19	0.21
$Re_\downarrow$	GGA	0.35	0.42	0.26	0.58	0.43
$Re_\downarrow$	GGA+*U*	0.36	0.43	0.26	0.61	0.45
$W_\uparrow$	GGA	0.18	0.16	0.18	0.15	0.15
$W_\uparrow$	GGA+*U*	0.17	0.14	0.18	0.13	0.14
$W_\downarrow$	GGA	0.20	0.22	0.18	0.30	0.24
$W_\downarrow$	GGA+*U*	0.21	0.23	0.18	0.34	0.25

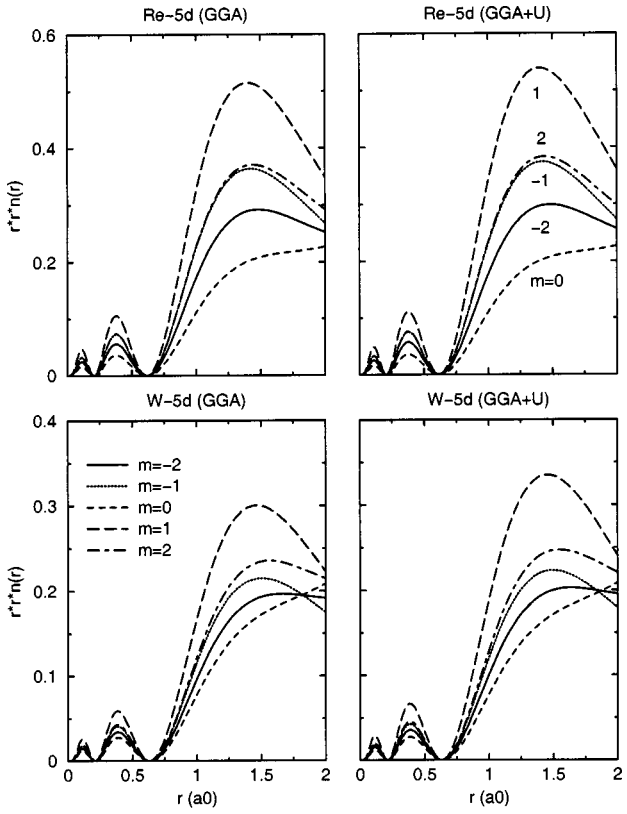

FIG. 6. Magnetic-orbital-decomposed charge densities of Re $5d$ and W $5d$ spin-down orbitals in Sr_2FeReO_6 (upper panels) and Sr_2CrWO_6 (lower panels), respectively.

enhances the differences between the fivefold magnetic orbitals and thus leads to stronger orbital polarizations and larger orbital magnetic moments for Re and W $5d$ orbitals.

IV. CONCLUSIONS

We have systematically investigated the electronic structures and magnetic properties of double perovskites Sr_2FeMoO_6, Sr_2FeReO_6, and Sr_2CrWO_6 by using the FP-LMTO method including spin-orbit interaction within the GGA, GGA+U, and also within the LSDA counterparts. The results demonstrate that the Fe-based double perovskites exhibit antiferromagnetic-coupling gaps, while the Cr-based double perovskite exhibits a crystal-field-splitting gap in the majority spin. In the meantime, the Fermi level lies in the minority-spin t_{2g} bands of hybridized d orbitals of transition-metal ions, resulting in a fully spin-polarized conductivity. The band gaps in the majority spins are dramatically enhanced by the on-site Coulomb energy U. On the other hand, the total spin moments of these compounds in ferrimagnetic half-metallic ground states are found to be 4, 3, and $2\mu_B$/f.u., respectively. The obtained spin moments are compatible with observed moments. The orbital moments of $3d$ elements Fe and Cr and of the $4d$ ion Mo are all quenched even though the on-site Coulomb energy U is taken into account. In contrast, the $5d$ ions W and Re exhibit large unquenched orbital moments even from the GGA and LSDA. The origin of the large orbital moments is attributed to the competition between the octahedral ligand field and the strong spin-orbit coupling in the $5d$ orbitals. Future experiments on spectra and magnetic moments would clarify the importance of U on these materials.

ACKNOWLEDGMENTS

This work was supported by the National Science Council of Taiwan (Grant Nos. NSC90-2119-M-007-004 and NSC90-2112-M-002-040).

[1] A. W. Sleight and R. Ward, J. Am. Chem. Soc. **83**, 1088 (1961); J. Longo and R. Ward, *ibid.* **83**, 2816 (1961); F. K. Patterson, C. W. Moeller, and R. Ward, Inorg. Chem. **2**, 196 (1963).
[2] M. T. Anderson, K. B. Greenwood, G. A. Taylor, and K. R. Poeppelmeier, Prog. Solid State Chem. **22**, 197 (1993).
[3] K. I. Kobayashi, T. Kimura, H. Sawada, K. Terakura, and Y. Tokura, Nature (London) **395**, 677 (1998).
[4] K. I. Kobayashi, T. Kimura, Y. Tomioka, H. Sawada, K. Terakura, and Y. Tokura, Phys. Rev. B **59**, 11 159 (1999).
[5] J. B. Philipp, D. Reisinger, M. Schonecke, A. Marx, A. Erb, L. Alff, R. Gross, and J. Klein, Appl. Phys. Lett. **79**, 3654 (2001).
[6] W. Westerburg, D. Reisinger, and G. Jakob, Phys. Rev. B **62**, R767 (2000).
[7] A. S. Ogale, S. B. Ogale, R. Ramesh, and T. Venkatesan, Appl. Phys. Lett. **75**, 537 (1999).
[8] D. D. Sarma, P. Mahadevan, T. S. Dasgupta, S. Ray, and A. Kumar, Phys. Rev. Lett. **85**, 2549 (2000).
[9] V. I. Anisimov, J. Zaanen, and O. K. Andersen, Phys. Rev. B **44**, 943 (1991).
[10] Z. Fang, K. Terakura, and Kanamori, Phys. Rev. B **63**, 180407 (2001); J. Kanamori and K. Terakura, J. Phys. Soc. Jpn. **70**, 1433 (2001).
[11] H. Wu, Phys. Rev. B **64**, 125126 (2001).
[12] S. Ray, A. Kumar, D. D. Sarma, R. Cimino, S. Turchini, S. Zennaro, and N. Zema, Phys. Rev. Lett. **87**, 097204 (2001).
[13] I. V. Solovyev, Phys. Rev. B **65**, 144446 (2002).
[14] S. Y. Savrasov, Phys. Rev. B **54**, 16 470 (1996).
[15] A. I. Liechtenstein, V. I. Anisimov, and J. Zaanen, Phys. Rev. B **52**, R5467 (1995).
[16] S. H. Vosko, L. Wilk, and M. Nusair, Can. J. Phys. **58**, 1200 (1980).
[17] J. P. Perdew, K. Burke, and M. Ernzerhof, Phys. Rev. Lett. **77**, 3865 (1996).
[18] A. W. Sleight, J. Longo, and R. Ward, Inorg. Chem. **1**, 245 (1962).
[19] Z. Zhang and S. Satpathy, Phys. Rev. B **44**, 13 319 (1991).
[20] M. A. Korotin, V. I. Anisimov, D. I. Khomskii, and G. A. Sawatzky, Phys. Rev. Lett. **80**, 4305 (1998).
[21] J. S. Kang, H. Han, B. W. Lee, C. G. Olson, S. W. Han, K. H. Kim, J. I. Jeong, J. H. Park, and B. I. Min, Phys. Rev. B **64**, 024429 (2001).
[22] C. Chmaissem, R. Kruk, B. Dabrowski, D. E. Brown, X. Xiong, S. Kolesnik, J. D. Jorgensen, and C. W. Kimball, Phys. Rev. B **62**, 14 197 (2000).
[23] J. Linden, T. Yamamoto, M. Karppinen, H. Yamauchi, and T. Pietari, Appl. Phys. Lett. **76**, 2925 (2000).
[24] B. Martinez, J. Navarro, L. Balcells, and J. Fontcuberta, J. Phys.: Condens. Matter **12**, 10515 (2000).
[25] C. Ritter, M. R. Ibarra, L. Morellon, J. Blasco, J. Garcia, and J. M. De Teresa, J. Phys.: Condens. Matter **12**, 8295 (2000).
[26] Y. Moritomo, S. Xu, A. Machida, T. Akimoto, E. Nishibori, M. Takata, and M. Sakata, Phys. Rev. B **61**, R7827 (2000).
[27] B. Garcia-Landa, C. Ritter, M. R. Ibarra, J. Blasco, P. A. Algarabel, R. Mahendiran, and J. Garcia, Solid State Commun. **110**, 435 (1999).
[28] I. V. Solovyev, A. I. Liechtenstein, and K. Terakura, Phys. Rev. Lett. **80**, 5758 (1998).
[29] V. I. Anisimov, I. S. Elfimov, N. Hamada, and K. Terakura, Phys. Rev. B **54**, 4387 (1996).
[30] S. K. Kwon and B. I. Min, Phys. Rev. B **62**, 73 (2000).
[31] H. T. Jeng and G. Y. Guo, J. Appl. Phys. **92**, 951 (2002); D. J. Huang, H. T. Jeng, C. F. Chang, G. Y. Guo, J. Chen, W. P. Wu, S. C. Chung, S. G. Shyu, C. C. Wu, H. J. Lin, and C. T. Chen, Phys. Rev. B **66**, 174440 (2002).